A Hybrid Thermoelectric Generator – Battery Power Supply System Toward Replacement-Free Battery

S. Tanabe[1], Y. Sakamoto[1], H. Uchida[2], T. Tanzawa[1]
[1] Shizuoka univ., Japan, [2] Zeon Corp., Japan

***Abstract*-- This study proposes a hybrid thermoelectric generator (TEG) – battery power supply system to achieve replacement-free batteries in sensor modules. A TEG is connected in series with the battery to increase the input voltage of a single DC-DC buck converter to drive a sensor IC and to return the majority of the battery power to the battery in every cycle. Experimental results show that the battery lifetime was extended by a factor of 9–84 with a 33 mH inductor and a small converter chip of 0.2 mm^2**

***Index Terms*—Battery, DC-DC converter, Replacement-free, Thermoelectric generator**

I. Introduction

When Internet of Things (IoT) sensing modules are placed in the field, they communicate with one another or cloud servers to collect the information around them and to keep society safe with little or no human intervention [1], [2]. However, there is the need to replace the battery used in the sensor modules. The cost of replacing old batteries with new ones has increased significantly as many sensor modules are distributed globally. To decrease the overall cost of sensor networks, technology is needed to eliminate battery replacement. Energy harvesting is a key technology for eliminating battery replacement. One solution is the use of an energy transducer (ET) to convert the surrounding energy, such as light, thermal flow, and vibration, into electric power for sensor modules without any battery [3], [4]. Because there is no battery, there is no need to replace batteries. However, when the modules require operation more often than the cycle time of the surrounding energy, a battery is required as a backup [5 – 8].

In [1], a battery charger was proposed for solar and thermoelectric energy harvesting. A boost converter stores charges in a storage capacitor first. When the capacitor voltage is above 1.8V, a switch is turned on to charge a battery from the storage capacitor. An over-charge protection circuit controls the switch. Maximum power point tracking circuit, oscillator, and state machine are implemented in a single die. Users need to place high resistance resistors to determine the detection voltages, which provides flexibility to the users and reduce the die size. 330nA quiescent current contributes to efficiency greater than 80% at a single cell solar voltage of 0.5V. In [2], a power management IC (PMIC) with integrated battery management and self-startup is developed for energy harvesting applications. It has three operation modes; energy transducer (ET)-to-Load, ET-to-battery and battery-to-load, depending on the states of load, ET and battery. DC-DC converter is configured as “boost” for the former two modes whereas as “buck” for the last one. The PMIC can manage wide operation conditions of an open circuit voltage of ET of 0.14-0.62V and battery voltage of 2.9-4.1V. The circuit requires an area of 2.4mm^2 in 180nm 1.8V/5V CMOS. In [3], thermoelectric energy harvesting system based on a reconfigurable TEG array is presented. TEG array has multiple sub-arrays of TEG. The numbers of TEG units connected in series and in parallel are determined depending on the open circuit voltage to extract the power from TEG array at maximum. The system generates internal power supplies of 1.2V and 2.7V for control circuits while charge the battery. The system was fabricated in 0.35μm CMOS with a silicon area of 4.5mm^2. The experimental result shows that a wide output power range of 38 μW–200 mW was realized with an input voltage from TEG arrays of 0.15 – 10.8 V. In [4], a reconfigurable DC-DC converter was developed for maximum TEG energy harvesting in a battery-powered wireless sensor node. It can be reconfigured in either one of the following four conditions; 1) single input dual output boost mode to drive the load and to charge battery from TEG in case that the TEG power is greater than the power required for the load, 2) battery-TEG pile-up buck mode to drive the load from the battery and TEG piled up or 3) dual-phase buck/boost to drive the load from TEG in a first period and from TEG and the battery piled up in a second period in case that the TEG power is lower than the power required for the load, and 4) battery-supplied buck mode in case that TEG does not generate power. The converter fabricated in 65nm CMOS required an area of 4mm^2.

Thus, the battery can supply power to the modules, when the energy transducer does not output sufficient power. Because such modules have both batteries and ETs, which increases the overall cost of the sensor network, the DC-DC converter for the battery and ET is needed in order to minimize the module size and cost. Consequently, our goal was to minimize the circuit area of the converter to be integrated into sensor/RF ICs.

II. Circuit concept

Figs. 1 (a), (b) illustrate the converter systems for a hybrid thermoelectric generator (TEG)–battery power supply. In a parallel connection [1], a buck/boost converter

is required for the battery to drive the load when the battery voltage V_{BAT} is higher or lower than the load voltage V_L owing to variation in V_{BAT}, whereas a boost converter is required for the TEG when *the* V_{EH} is always lower than V_L. As a result, two configurations are required when the battery and TEG are connected parallel to the load. In the proposed converter system for a hybrid TEG - battery power supply, the battery and TEG are connected in series to the buck converter [9 – 12]. When the sum of V_{BAT} and V_{EH} is always higher than V_L, the system only needs a single buck converter, which can contribute to cost reduction when the circuit is too small to be integrated into a sensor/RF IC. Some of the power converted by the buck converter is supplied to the load, and the remaining power is returned to the battery to extend the battery lifetime.

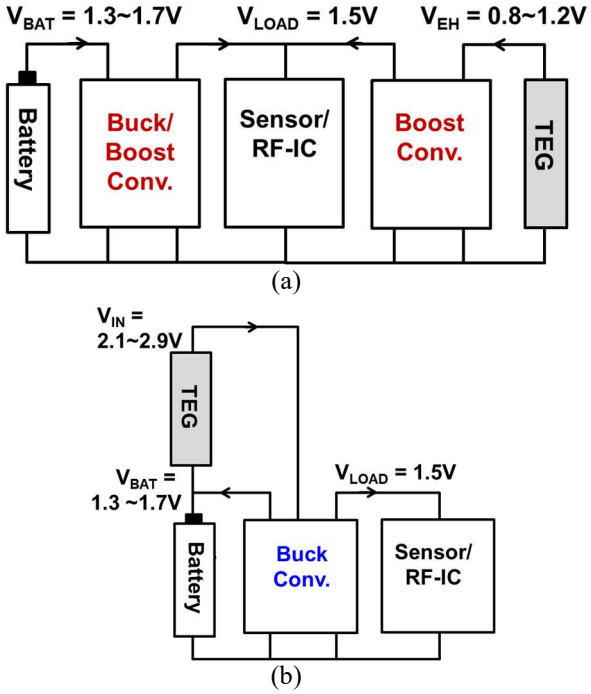

Fig. 1 DC-DC converter for hybrid thermoelectric generator - battery power supply; (a) conceptual parallel connection and (b) proposed serial connection.

Fig. 2 shows the detailed configuration to realize the concept of the proposed circuit. The capacitance values of C_I and C_O are selected to ensure that there are sufficiently small ripples at V_{IN} and V_L, respectively. The power converter has one input terminal and two output terminals. The input power P_{IN} is the sum of the output power of the battery (P_{BO}) and the effective power of the ET (P_E). Some of the output power of the converter is supplied to the load with *the* P_L. The remaining power, namely P_{BR}, is returned to the battery. The amount by which the battery lifetime could be extended is indicated by the battery lifetime extension (BLE) using P_L/P_B, where P_B is the effective battery power given by $P_{BO} - P_{BR}$. Thus, the BLE indicates the battery power savings that can be realized using the proposed converter system.

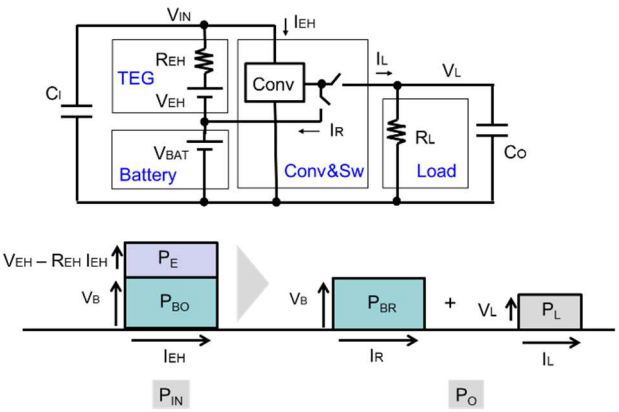

Fig. 2 Block diagram of the proposed converter system and breakdown of P_{IN} and P_O.

III. Circuit Design

Fig. 3 illustrates a circuit diagram of the proposed concept and waveform of the control signals and the resultant current. The circuit operates in discontinuous conduction mode to improve the power conversion efficiency at light loads [13].

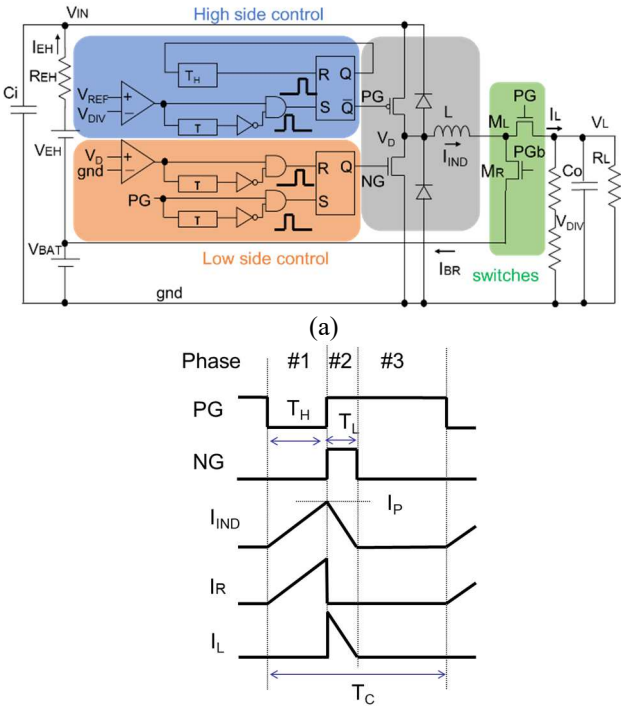

Fig. 3 (a) circuit diagram to realize the proposed concept and (b) waveform of the control signals and current components.

The load voltage V_L decreases owing to the load current. When V_{DIV} (a divided voltage of V_L) reaches a reference voltage V_{REF}, phase #1 starts with PG being low. During phase #1, the high side of the converter and the return path M_R are turned on. The inductor current I_{IND} returns to the battery, as shown by I_{BR}. After a predetermined interval (T_H) is passed, phase #2 starts with NG being high. The low side of the converter and the load

switch (M_L) are turned on to discharge I_{IND} into the load. When the drain voltage of the low-side NMOS (V_D) reaches ground level, all switches are turned off. In phase #3, the input and output capacitors C_I and C_O are charged via R_{EH} and discharged via R_L, respectively. To allow the converter circuit, except for the inductor, to be integrated into sensor/RF ICs, the minimum load current is limited to 100 µA. As a result, relatively small transistors are acceptable, which could contribute to a high-power conversion efficiency, especially under light loads. In this design, additional circuits such as an overcharging protection circuit and maximum power point tracking were not included, which will be needed for production. This paper focuses on the main circuit.

Fig. 4 describes loop current components in phases #1 – 3. Input and output sides have steady current flows. The output capacitor C_O is discharged to the load. The input capacitor C_I is charged from the series power source of the battery and TEG. This current component is the discharging current from the battery. A part of the charges stored in C_I returns to the battery in phase #1. This current component is the charging current to the battery. When those discharging and charging currents are balanced on average, a net discharging current can be limited. The energy stored in the inductor in phase #1 is transferred to the load in phase #2. The load current in phases #1 - 3 is compensated with the charging current in phase #2.

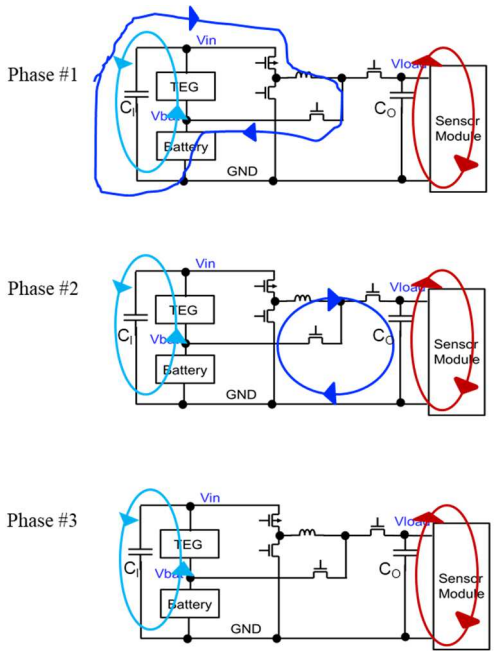

Fig. 4 Loop current components in phases #1 – 3.

Circuit equations to design the circuit are given as follows, assuming that power supply capacitors C_I and C_O are large enough to be able to ignore ripples in V_{IN} and V_L. V_{IN} is determined by (1).

$$V_{IN} = V_{EH} + V_{BAT} - R_{EH}I_{EH} \quad (1)$$

The average current returning to the battery per cycle I_{BR} and the average load current I_L are determined by (2) and (3), respectively, using the peak inductor current I_P.

$$I_{BR} = \frac{I_P T_H}{2T_C} \quad (2)$$

$$I_L = \frac{I_P T_L}{2T_C} \quad (3)$$

Equations (4) and (5) are obtained with a linear approximation in I_{IND} and an assumption that effective inductor voltages in phases #1 and #2 are given by RHS,

$$L\frac{I_P}{T_H} = V_{IN} - V_{BAT} - R_P I_P \quad (4)$$

$$L\frac{I_P}{T_L} = V_L + R_N I_P \quad (5)$$

The effective resistance R_P and R_N in high and low sides are assumed to be (6) and (7), respectively, where R_{DS1} and R_{DS2} are on-resistance of MOSFETs in phases #1 and #2, and R_{IND} is resistance of the inductor.

$$R_P = (R_{DS1} + R_{IND})/2 \quad (6)$$

$$R_N = (R_{DS2} + R_{IND})/2 \quad (7)$$

Because a constant current I_{EH} is charged up C_I and the charges stored in C_I return to the battery or are consumed by the control circuit, (8) holds between I_{BR} and I_{EH}, where the current consumption in the control circuit I_{CKT} is given by DC and transient current as (9).

$$I_{BR} = I_{EH} - I_{CKT} \quad (8)$$

$$I_{CKT} = I_{CKT-DC} + \frac{C_G V_{IN}}{T_C} \quad (9)$$

DC current $I_{CKT\text{-}DC}$ includes the current flowing in current reference, comparators and delay circuits. C_G indicates the total gate capacitance including switching MOSFETs and the control circuits operating once per cycle.

Circuit valuables are determined as follows. Starting with selection of the inductor, one can have the values of L and R_{IND}. For a given T_H, I_P is determined by (4). Equation (5) provides T_L. T_C is determined as a function of I_L via (3). I_{BR} is calculated by (2). Equations (8) and (9) give I_{EH}. Finally, V_{IN} is determined by (1).

Circuit performance can be presented by the battery lifetime extension *BLE* and power conversion efficiency of the DC-DC converter η, respectively given by (10) and (11). Note that the output current of the battery I_{BAT} is equal to I_{EH}, resulting in a net output current of I_{CKT}.

$$BLE = \frac{P_{CONV}}{P_{PROP}} = \frac{I_L \times V_L}{I_{BAT} \times V_{BAT}} = \frac{I_L \times V_L}{I_{CKT} \times V_B} \quad (10)$$

$$\eta = \frac{P_{OUT}}{P_{IN}} = \frac{V_L I_L + V_{BAT} I_{BR}}{V_{IN} I_{IN}} \quad (11)$$

Design parameters in Table I are used for demonstrating the design concept.

TABLE I
DESIGN PARAMETERS FOR DEMONSTRATION

PARAMETERS	VALUES
V_{BAT} [V]	1.4, 1.56, 1.72
V_{EH} [V]	1.14, 1.24, 1.46
V_L [V]	1.52
R_{EH} [Ω]	1.2K
T_H [μs]	50
L [MH]	33
R_L [Ω]	20K – 50K
C_i [NF]	330
C_o [NF]	830
R_{IND} [Ω]	90
$R_{DS1} = R_{DS2}$ [Ω]	50
I_{CKT-DC} [μA]	1.0
C_G [PF]	400

IV. MEASUREMENT

The proposed circuit was fabricated in a standard 180 nm 1.8 V CMOS with no low-Vt transistors and with 3 V transistors for I/O, as shown in Fig. 5(a). In a measurement setup (Fig. 5(b)), the converter was connected to a flexible TEG [14] placed on a mimic thermal pipe and a 1.6 V Ni-Zn battery. The temperature of the thermal pipe was varied to vary V_{EH}. The output voltage of the battery was varied by adjusting the state of charge SOC. Fig. 5(c) shows the measured waveform at V_{BAT} = 1.56 V, V_{EH} = 1.24 V, and R_L = 50 kΩ. The peak inductor current was approximately 2 mA.

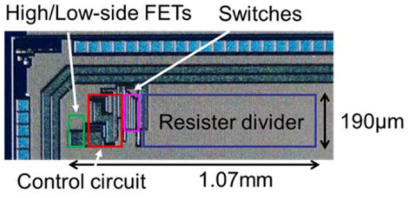

(a)

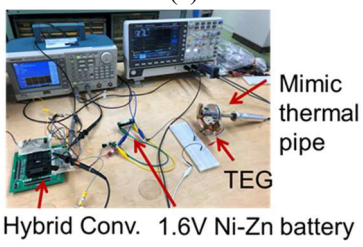

(b)

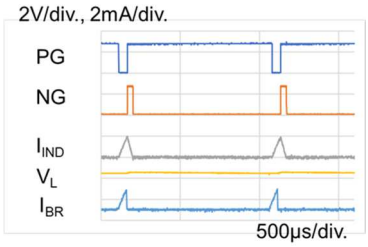

(c)

Fig. 5 (a) Chip micrograph, (b) measurement set-up, and (c) measured waveform.

BLE and η were measured against I_L, V_{BAT}, and V_{EH}, as shown in Fig. 6. In addition to the system shown in Fig. 5(b), another measurement setup was used with DC voltage sources for V_{BAT} and V_{EH}, and a resistor for R_{EH}, as shown by "m.dc" in Fig. 6. Theoretically, BLE increases as I_L or V_{EH} increases or as I_{BAT} decreases. Among all the combinations of R_L, V_{BAT}, and V_{EH}, as shown in Table I. the circuit achieved a BLE value ranging from 9–84 and a η value ranging from 84–91%.

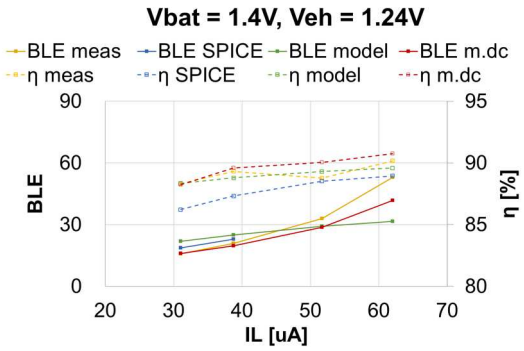

(a)

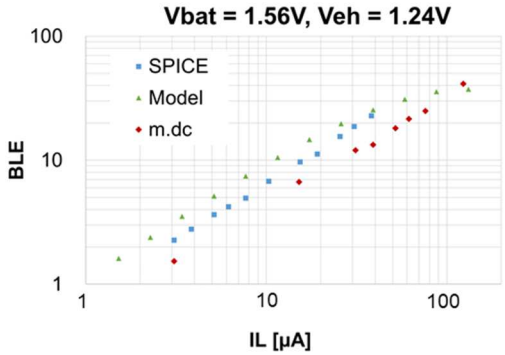

(b)

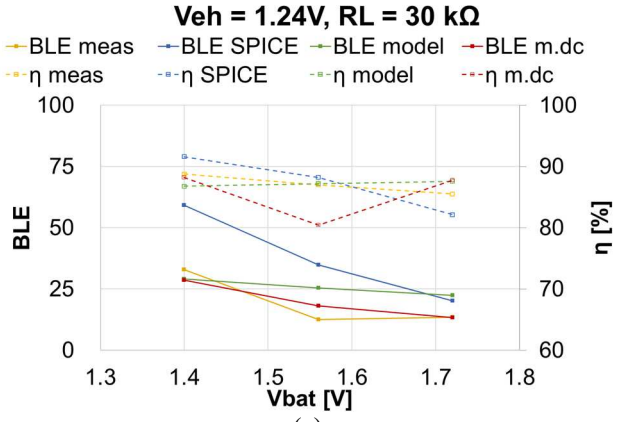

(c)

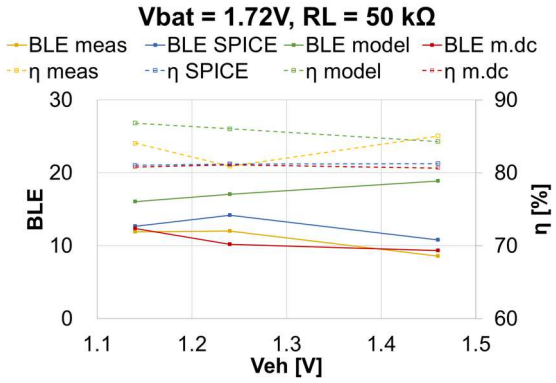

(d)

TABLE II
COMPARISON WITH THE PREVIOUS WORKS

	Design params	Kadirvel, ISSCC, 2012 [5]	Damak, JSSC, 2016 [6]	Wan, JSSC, 2019 [7]	Noh, ISSCC, 2021 [8]	This work
TEG	V_{EH}	>0.33V	0.14-0.62V	0.6 – 1.0V (*1)	0.1 - 0.5V	1.1-1.5V
	R_{EH}	N.A.	N. A.	1.5kΩ (*1)	8Ω	1.2kΩ
	P_{MAX} (=$V_{EH}^2/4/R_{EH}$)	N.A.	N. A.	3.6 – 10 mW	0.3 - 7.8mW	0.3 – 0.5mW
Load	V_L	3V	1V	1.2V, 2.7V	0.9-1.1V	1.55V
	I_L	10μA-40mA	10n-1μA	30μA - 60mA	1-20mA	1μA-100μA
Battery	V_{BAT}	3.3V	2.9-4.1V	3.6V	0.9-1.4V	1.4-1.7V
Conv.	Buck/Boost	Boost-only	Buck and Boost (Reconfigurable)	Reconfigurable. TEG arrays w/ charge pump back-up	Buck and Boost (Reconfigurable)	Buck-only
	Functions	TEG-to-CAP, CAP-to-BAT	ET-to-load, ET-to-BAT, Bat-to-load	Reconfigurable TEG-to-load, Reconfigurable TEG-to-BAT, BAT-to-load	TEG-to-load, TEG+BAT-to-load, BAT-to-load	TEG+BAT-to-load / BAT in every cycle
	Energy conversion device	Inductor	Inductor	None (Capacitors in charge pump)	Inductor	Inductor
	BLE	N.A.	N.A.	N.A.	N.A.	9 - 84
	Power conversion efficiency	80-90%	80-87%	86-99%	88.5% (Boost), 93.3% (Buck)	84-91%
	MPPT?	Y	Y	Y	Y	N
	CMOS	N.A.	180nm	350nm	65nm	180nm
	Low-Vt transistor?	Y	Y	N	Y	N
	Circuit area	N.A.	2.4mm^2	4.5mm^2	4mm^2	0.2mm^2

(*1) each of 60 TEG units

Fig. 6 Measured results; BLE and as a function of (a), (b) I_L, (c) V_{BAT}, and (d) V_{EH}.

V. COMPARISON WITH PREVIOUS WORKS

Table II compares the performance of the proposed design with those of previous works [5 – 8], where P_{MAX} is the estimated maximum attainable power for each ET. Because an application of this work is to IoT sensor modules with an average power consumption of the order of 10 μW, even relatively small transistors can drive the load. When the output power is greater than 100 μA, the converter stops working because it cannot operate in DCM. Thus, the circuit can be designed with a silicon area of 0.2 mm^2, which is small enough to be implemented in sensor/RF ICs. Note that bandgap reference is not included in the size of the circuit assuming that the sensor/RF ICs has a reference circuit. Low threshold voltage transistors are not needed because the converter operates with a voltage higher than 2 V owing to the series connection of the battery and TEG. Therefore, a standard 180 nm 1.8 V CMOS with no low-Vt transistors and with 3 V transistors for I/O was sufficient to realize the proposed DC-DC converter for a hybrid TEG–battery power supply. As a result, the proposed converter will contribute to the development of low-cost and small-size sensor modules. In this initial circuit design, maximum power point tracking was not implemented, which is theoretically given by the condition of $V_{IN} = V_{BAT} + V_{EH}/2$.

VI. CONCLUSIONS

A hybrid thermoelectric generator (TEG) - battery power supply system was proposed toward replacement-free battery. TEG and battery were connected in series.

Thus, only a DC-DC buck converter was required. The power extracted from TEG was delivered into the load and returned into the battery in every operation cycle. The proposed circuit was fabricated in a standard 180nm CMOS based on the design equations. Experimental results show that the battery lifetime was extended by a factor of 9–84 with a 33 mH inductor and a small converter chip of 0.2 mm^2.

ACKNOWLEDGMENT

This work was supported by Zeon Corp., d.lab-VDEC, Synopsys, Inc., and Cadence Design Systems, Inc.

REFERENCES

[1] A. Zanella, N. Bui, A. Castellani et al., “Internet of Things for smart cities,” IEEE Internet of Things Journal, vol. 1, no. 1, pp. 22–32, Feb. 2014.

[2] A. Al-Fuqaha, M. Guizani, M. Mohammadi et al., “Internet of things: A survey on enabling technologies, protocols, and applications,” IEEE Communications Surveys & Tutorials, vol. 17, no. 4, pp. 2347–2376, 2015.

[3] P. D. Mitcheson, E. M. Yeatman, G. K. Rao et al., “Energy harvesting from human and machine motion for wireless electronic devices,” Proc. IEEE, vol. 96, no. 9, pp. 1457–1486, Sep. 2008.

[4] S. Sudevalayam and P. Kulkarni, “Energy harvesting sensor nodes: Survey and implications,” IEEE Commun. Surveys Tuts., vol. 13, no. 3, pp. 443–461, 3rd Quater 2011.

[5] K. Kadirvel, Y. Ramadass, U. Lyles et al., “A 330nA Energy-Harvesting Charger with Battery Management for Solar and Thermoelectric Energy Harvesting,” *ISSCC*, pp. 106 - 107, Feb. 2012.

[6] D. El-Damak and A. P. Chandrakasan, “A 10 nW–1 µW Power Management IC With Integrated Battery Management and Self-Startup for Energy Harvesting Applications,” *IEEE JSSC,* vol. 51, no. 4, pp. 943 - 954, Apr. 2016.

[7] Q. Wan and P. K. T. Mok, “A 14-nA, highly efficient triple-output thermoelectric energy harvesting system based on a reconfigurable TEG array,” *IEEE JSSC,* vol. 54, no. 6, pp. 1720 - 1732, Jun. 2019.

[8] Y. S. Noh, J. I. Seo, W. J. Choi et al., “A Reconfigurable DC-DC Converter for Maximum TEG Energy Harvesting in a Battery-Powered Wireless Sensor Node,” *ISSCC*, pp. 266 - 267, Feb. 2021.

[9] Y. Sakamoto, H. Uchida, T. Tanzawa, “A Power Converter System for Energy Harvesting Toward Zero Net Battery Power,” IEICE general conference, C-12-20, Mar. 2020.

[10] Y. Sakamoto, T. Tanzawa, "A Design of DC-DC Converter for Thermoelectric Energy Harvesting with Battery Backup," IEICE society conf., C-12-1, Sep. 2021.

[11] S. Tanabe, Y. Sakamoto, T. Tanzawa, "Modeling of Buck converter for TEG-Battery hybrid system," IEICE general conference, C-12-20, Mar. 2022.

[12] S. Tanabe, Y. Sakamoto, T. Tanzawa, "Evaluation of DC/DC converter for hybrid power supply of thermoelectric generator and battery," C-12-2, Sep. 2022.

[13] B. Arbetter; R. Erickson; D. Maksimovic, “DC-DC converter design for battery-operated systems,” *PESC*, pp. 103 - 109, Jun. 1995.

[14] K. Suemori, S. Hoshino, T. Kamata, “Flexible and lightweight thermoelectric generators composed of carbon nanotube—polystyrene composites printed on film substrate,” *Appl. Phys. Lett.* **2013**, *103*, 153902.